


# Morphological characterization of the novel fine structure of the PMMA/PVDF blend

著者	Akihiro Naruke, Xiaobin Liang, Ken Nakajima, Toshio Nishi
journal or publication title	Polymer Journal
volume	54
page range	783–792
year	03 March 2022
出版社	Springer Nature
権利	This version of the article has been accepted for publication, after peer review (when applicable) and is subject to Springer Nature's AM terms of use, but is not the Version of Record and does not reflect post-acceptance improvements, or any corrections. The Version of Record is available online at: <a href="http://dx.doi.org/10.1038/s41428-022-00625-z">http://dx.doi.org/10.1038/s41428-022-00625-z</a>
URL	<a href="https://research.konicaminolta.com/jp/report/">https://research.konicaminolta.com/jp/report/</a>

doi: /10.1038/s41428-022-00625-z



# Morphological characterization of the novel fine structure of the PMMA/PVDF blend

Akihiro Naruke<sup>1,2</sup> · Xiaobin Liang<sup>1</sup> · Ken Nakajima <sup>1</sup> · Toshio Nishi<sup>3</sup>

Received: 2 December 2021 / Revised: 7 January 2022 / Accepted: 15 January 2022  
© The Society of Polymer Science, Japan 2022

## Abstract

Poly(methyl methacrylate) (PMMA)/Poly(vinylidene fluoride) (PVDF) blends are well known as polymer pairs with unique and complex properties. Using low voltage scanning transmission electron microscopy (LV-STEM), we found that there were previously unseen nanoscale structures inside them. The heterogeneous structures in the blends were formed on the same scale that did not deviate from the size of a single molecular chain, regardless of the solution casting, melt mixing, mixing ratios, and even amorphous or crystalline state of PVDF. The characteristics of these structures were discussed in accordance with thermophysical properties and intermolecular interaction properties, which provides the following new findings for the first time. First, the mixing ratio-dependent melting point depression exhibited by PMMA/PVDF blends is due to the size of their interface region. Second, the complex thermophysical behavior of the solution-casting blends is caused by the presence of ultrafine PVDF crystals. Finally, LV-STEM visualized the molecular miscibility of PMMA and PVDF in the melt-mixing samples.

## Introduction

Polymer blends, in which crystalline polymers are added to amorphous polymer matrices, have been applied to various products because of their ability to impart a sharp change in physical properties due to the phase transition of the crystalline polymers while maintaining the high dimensional stability of the amorphous polymer matrices. Here, physical properties mean, for example, viscosity change due to heat. One example among industrial products is the toner used in multifunction printers. The purpose of adding crystalline

polymers is to melt the toner in a short period of time and to fix it to the paper, thereby achieving excellent energy-saving effects [1]. To spread the effect of the added crystalline polymer throughout the blend, crystalline polymers should be finely dispersed in the amorphous polymer matrix on the order of nanometers. Therefore, for appropriate material design, it is preferable to use polymer pairs that exhibit miscibility in the molten state. In other words, we should aim to design materials in such a way that a compatible solid-state is derived from a miscible molten state.

On the other hand, when the crystalline polymer is a minor component in such miscible crystalline/amorphous polymer blends, the behavior of the crystalline polymer is extremely unstable, which makes stable manufacture and storage of products difficult. The low stability of such blends is mainly due to the following two factors. One is the change in the state of crystalline polymers, including their presence in an amorphous state. Another is the melting temperature of the crystalline polymer, which considerably varies depending on the mixing ratio. In the past and currently, these compounds have been frequently studied using poly(methyl methacrylate) (PMMA) and poly(vinylidene fluoride) (PVDF) blends [2–5]. For example, it is well-known that PVDF exists in an amorphous state in PMMA/PVDF blends obtained by melt mixing when the ratio of PVDF is less than 50 weight% [2]. It is also known that the

---

**Supplementary information** The online version contains supplementary material available at <https://doi.org/10.1038/s41428-022-00625-z>.

✉ Ken Nakajima  
nakajima.k.aa@m.titech.ac.jp

- <sup>1</sup> School of Materials and Chemical Technology, Tokyo Institute of Technology, 2-12-1 O-okayama, Meguro-ku, Tokyo 152-8552, Japan
- <sup>2</sup> Advanced Technology Center, Corporate R&D Headquarters, KONICA MINOLTA, INC., No.1 Sakura-machi, Hino-shi, Tokyo 191-8511, Japan
- <sup>3</sup> Tokyo Institute of Technology, Meguro-Ku, Tokyo 152-8552, Japan

melting point of PVDF is considerably lower than that of pure PVDF in blends where PVDF is fully crystallized by cast blending and that the degree of melting point depression depends on the ratio of PVDF [3]. In addition, the compatibility and/or miscibility of the two polymer pairs, as well as the crystallization behavior of PVDF, depend on the three crystal forms ( $\alpha$ ,  $\beta$ ,  $\gamma$ ) of PVDF and the difference in the tacticity of PMMA [6–8].

These peculiar behaviors of PMMA/PVDF blends have been analyzed using various techniques, including the analysis of the crystalline state of PVDF using thermal analysis and X-ray diffraction measurements, morphological considerations using optical microscopy, and interpretation of the rheological properties of blends [9–15]. In addition to these evaluation methods, analysis from a detailed perspective has been actively performed. It is difficult to interpret PMMA/PVDF, which is believed to exhibit molecular miscibility, only by macroscopic analysis, which inevitably requires analysis and discussion at the molecular scale. Such evaluation methods are mainly related to the intermolecular interactions between PMMA and PVDF, and the following three are examples. The first is the evaluation of molecular mobility by measuring the relaxation time using pulsed nuclear magnetic resonance [16, 17]. The second is the analysis of the hydrogen bonding between the carbonyl group of PMMA and polar units of PVDF by Fourier transform infrared spectroscopy (FT-IR) [18–20]. The third is the evaluation of the mobility of the PMMA side chain by dielectric relaxation [21, 22]. For morphological evaluation, which is important for interpreting phenomena, only macro- to microscale observation methods have been used. This refers, for example, to the observation of spherulites by polarized optical microscopy [10] or by scanning electron microscopy [23]. These approaches are used because most of the previous studies have focused on PVDF-rich blends, in which PVDF crystallizes relatively stably. Therefore, PVDF formed a large spherulitic structure in the blends, and morphological analysis was sufficiently conducted by the abovementioned microscopes. However, based on the abovementioned background, focusing on PVDF-poor blends where PVDF is unstable and macroscopic spherulites cannot be identified, morphological analysis at the nanoscale becomes necessary. However, few such studies have been conducted to date.

We believe that one of the factors governing the complex behavior of PMMA/PVDF blends is the internal structure at the nanoscale, which has not been observed thus far, and one of the objectives of this study is to visualize it. Polymer blends that exhibit miscibility, such as PMMA/PVDF, form solid blends from molecularly mixed states. A variety of state-of-the-art microscopes are candidates for observing nanoscale microstructures. Among them, we chose electron microscopy, especially low voltage scanning transmission electron microscopy (LV-STEM). LV-STEM, due to its low acceleration

voltage, can provide imaging by thermal diffuse scattering, which is an advantage for contrast generation between light elements [24]. Additionally, it is not necessary to use pre-treatments such as heavy metal staining or removing one material by dry or wet etching, which sometimes destroy the original structures of the samples. Moreover, knock-on damage caused by a high acceleration voltage, which is often a concern with fluoropolymers such as PVDF, can be reduced.

In this study, LV-STEM was used to observe the internal structures of PMMA/PVDF blends for the first time. The obtained images were discussed in relation to the physical properties of the blends. Specifically, the melting point depression of PVDF crystals in PMMA/PVDF blends, which has been extensively studied in the past, was discussed based on these internal structures. Moreover, we also added new insights into the complex melting behaviors of the blends, which cannot be expressed only by the melting point depression. These were also explained as the intermolecular interactions between PMMA and PVDF.

## Materials and methods/experimental procedure

### Materials and sample preparation

PVDF (average  $M_w$  ~120,000) and PMMA (average  $M_w$  ~534,000) in pellet form were purchased from Merck KGaA, Germany. Throughout this paper, the ratio of PVDF in the blend is reported on a weight basis. The solution-casting PMMA/PVDF blends in film form were cast from *N,N*-dimethylformamide (DMF) solution onto a glass surface at room temperature. The initial concentration of each polymer in DMF was ~3 g/100 mL. After the mixtures were cast, DMF was allowed to evaporate very slowly under a stream of air at reduced pressure (34 kPa) for at least 1 week. The resulting films were subjected to further drying under vacuum at room temperature for 1 week as previously reported [3]. The melt-mixing PMMA/PVDF blends were produced with a twin-screw kneader using DSM Xplore, Netherlands Model MC 5 at 200 °C. Considering that the state of the blend, especially the amorphous-crystalline states of PVDF, can be changed depending on the cooling conditions, the melt-mixed strands were cooled by leaving at room temperature or quenching with ice water.

### Measurement of thermal properties

Thermal analysis by DSC was performed using Hitachi High-Tech Science Corporation, Japan Model EXTAR 6000, at 10 °C/min temperature increase condition. A previous study [3] reported that the melting temperature of PVDF crystals in PMMA/PVDF blends decreased as the

weight fraction of PVDF decreased and that the melting point depression that generally occurred in amorphous-crystalline polymer blends was expressed as Eq. (1),

$$\frac{1}{T_{m^0}(\text{blend})} - \frac{1}{T_{m^0}(\text{pure})} = -\frac{RV_2}{\Delta H^0 V_1} \left[ \frac{\ln \phi_2}{m_2} + \left( \frac{1}{m_2} - \frac{1}{m_1} \right) \phi_1 + \chi_{12} \phi_1^2 \right] \quad (1)$$

where  $T_{m^0}(\text{blend})$  and  $T_{m^0}(\text{pure})$  are the equilibrium melting points of the blend and of the pure crystallizable component, respectively.  $\Delta H^0$  is the heat of fusion of the perfectly crystallizable polymer per mole of the repeat unit,  $V$  is the molar volume of the repeating units of the polymers,  $m$  is the degree of polymerization, and  $\phi$  is the volume fraction of the component in the blend. Subscripts 1 and 2 refer to the amorphous and crystalline polymers, respectively.  $R$  is the universal gas constant, and  $\chi_{12}$  is the polymer–polymer interaction parameter. However, of note, these are considerations of the melting point depression, or melting behavior, from a thermodynamic point of view and do not include considerations from a morphological point of view.

## Visualization of morphology

The internal structure was visualized with STEM using Hitachi High-Tech Corporation, Japan Model S-4800 at an accelerating voltage of 30 kV. Samples for observation were obtained using a Leica Microsystems GmbH, Germany Model UC-6 ultramicrotome to prepare thin sections of ~100 nm thickness at room temperature.

## Evaluation of interactivity

The miscibility of PMMA and PVDF in the melt state accounts for the hydrogen bonding between the C=O carbonyl group of PMMA and the CH<sub>2</sub> unit of PVDF [18, 19]. The presence or absence and the degree of hydrogen bonding can be evaluated by observing the C=O peak of PMMA obtained by FT-IR measurements. If hydrogen bonding is formed, this peak is shifted to a lower wavenumber due to the vibration limitation caused by the bonding. This was measured by attenuated total reflection (ATR)/FT-IR (Thermo Fisher Scientific, USA Model AVATAR 370) with Ge prism at a wavenumber resolution of 1 cm<sup>-1</sup>.

## Results

### Solution-casting samples

Figure 1 shows thermograms of the solution-casting blends of PMMA/PVDF with various mixing ratios and pure PVDF measured at a heating rate of 10 °C/min. Endothermic peaks from the melting of crystalline PVDF were observed in all

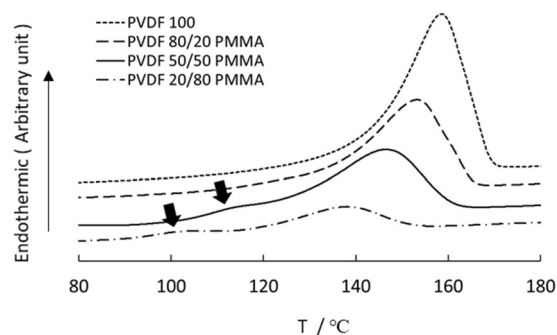


**Fig. 1** Thermograms of solution-casting PVDF and PMMA/PVDF blends with various mixing ratios obtained at a heating rate of 10 °C/min. The arrows indicate the low-temperature melting peaks that we are focusing on

blends, including blends with low PVDF ratios. The melting curves were shifted toward lower temperatures with decreasing PVDF ratio while maintaining their shapes. However, of note, in the blends with a low PVDF ratio, the presence of small peaks at lower temperatures than the main melting peak was evident. Specifically, those peaks exist at temperature that is slightly higher than 100 °C for the blend with PVDF 20% and at temperature that is slightly higher than 110 °C for the blend with PVDF 50%, as indicated by the arrows. These small endothermic peaks were also observed in a previous study [3], while their origin was not discussed. Thus, we added a detailed consideration to this information in “Discussion” section. Figures 2 and 3 show how the melting temperature  $T_m$  and total endothermic area due to the melting of crystalline PVDF depend on the weight fraction of PVDF in the blends. The data from the previous study [3] were also superimposed in the figures. The melting point is determined by the well-established method [25], which identifies the temperature at which the last detectable traces of crystalline nature disappear upon heating. The dashed line in Fig. 4 represents a marginal case where there is no interaction between the components and PVDF is assumed to be fully crystallized from the blend. The proximity of the plot of measurements to this dashed line indicates that nearly all crystallizable PVDF in the blend is crystallized. The plots of the melting point of pure PVDF and the melting point depression of the blends and the endothermic area close to the dashed line shown in Figs. 2 and 3 replicate the results of the previous study [3]. The melting enthalpy of pure PVDF in this experiment was 58.1 J/g, which agrees well with the previous study [26]. The melting point depression of PVDF crystals in blends is the direct consequence of the negative value of the interaction parameter  $\chi_{12}$  shown in Eq. (1) [3]. Equation (1) is often used to determine the miscibility of polymer pairs, and there are many studies on this subject [27–30].

Figure 4 shows cross-sectional STEM bright-field images of the blends with various mixing ratios. The dark

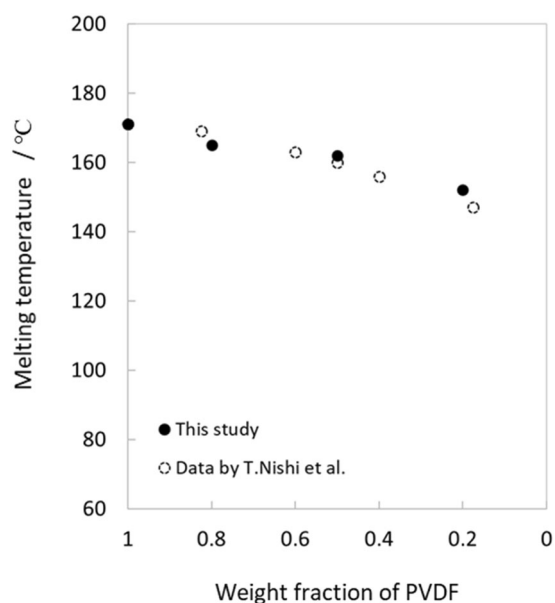


**Fig. 2** Dependence of melting temperature ( $T_m$ ) of the solution-casting blends on the weight fraction of PVDF. The black dots are the data from this study, and the dots made of white dotted lines are the data by Nishi et al. [3]

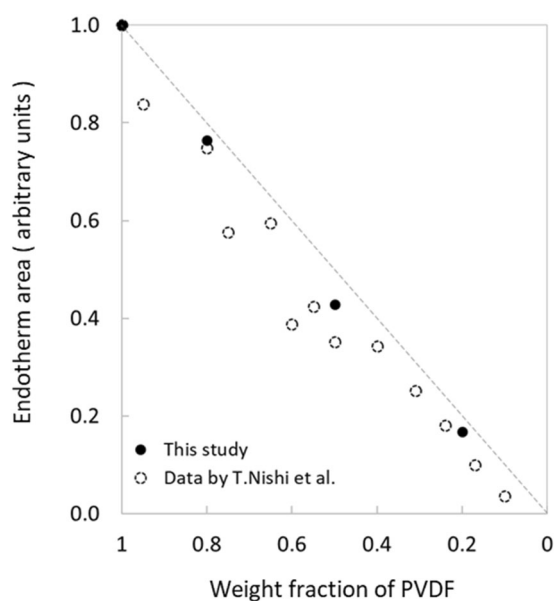


**Fig. 3** Dependence of the endotherm area due to the melting of PVDF crystals in the solution-casting blends on the weight fraction of PVDF. The black dots are the data from this study, and the dots made of white dotted lines are the data by Nishi et al [3]

contrasts in the image are crystalline PVDF domains, indicating the presence of nanoscale fine structures inside the blends that are considerably smaller than the  $0.5\ \mu\text{m}$  scale bar. Specifically, when the PVDF ratio was 20%, crystalline PVDF formed islands  $\sim 200\ \text{nm}$  in diameter, and when the ratio was 50%, the PVDF crystalline islands were interconnected. In the case of the ratio of 80%, the PVDF crystals dominate the field of view. In this study, the

contrast between PVDF crystals and amorphous PMMA domains was successfully obtained using LV-STEM with an acceleration voltage of 30 kV, without the use of pre-treatment methods such as heavy metal staining or etching.

### Melt-mixing samples

Figure 5 shows the internal structures of melt-mixing blends with PVDF 50 and 20% produced under several different cooling conditions. Cooling at  $-20\ ^\circ\text{C}/\text{min}$  means that samples of melt mixing were held at  $200\ ^\circ\text{C}$  for 30 min in the DSC pan and then cooled at  $-20\ ^\circ\text{C}/\text{min}$  using the DSC program. Here, no endothermic peaks were observed in the DSC measurements of any blends (see Fig. S1 in Supplementary Information). Thus, all PVDF of any blends existed in an amorphous state. Figure 5 shows that fine sea-island structures are formed in all blends. The size of the islands is approximately 300 nm in diameter, and there is no change in size between blends with PVDF ratios of 50 and 20%, nor is there any change in the structure with cooling conditions. We will mention in more detail in the discussion section the nature of the islands with dark contrast, but they are judged to be PMMA/PVDF mixtures with a higher PVDF ratio than the sea region.

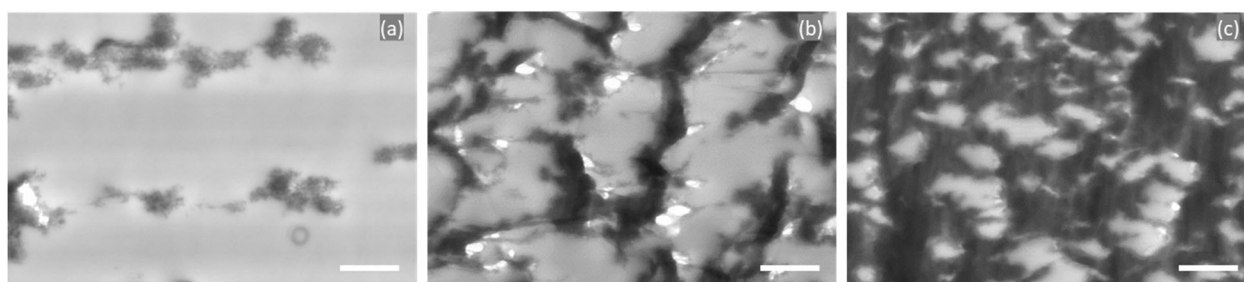
### FT-IR measurement of solution-casting and melt-mixing samples

Figure 6 shows the absorbance of the C=O band of the carbonyl group of PMMA in blends prepared by solution casting and melt mixing with a PVDF ratio of 50%, obtained by FT-IR measurements. As mentioned above, when PMMA and PVDF interact to form hydrogen bonds, this peak shifts to a lower wavenumber, and it is known that hydrogen bonding is generated only when PVDF is in the amorphous state [18]. Figure 6 shows that, compared to the pure PMMA peak shown in the dotted line, there was no shift in the solution-casting blend shown in the solid line, whereas the melt-mixing blend shown in the dashed line showed a shift to a lower wavenumber, indicating the formation of hydrogen bonding. This is consistent with the result of the DSC measurement in this study, i.e., only crystalline PVDF exists in the solution-casting blends, and only amorphous PVDF exists in the melt-mixing blends.

## Discussion

### Solution-casting samples

First, we consider the melting point depression derived by the Nishi-Wang equation from a morphological point of view. In Eq. (1), the degree of melting point depression on



**Fig. 4** STEM bright-field images of solution-casting PVDF/PMMA blends in various mixing ratio. **a** 20/80, **b** 50/50, **c** 80/20. Scale bar is 0.5  $\mu\text{m}$

**Fig. 5** STEM bright-field images of melt-mixing PMMA/PVDF blends by various cooling processes from melting at 200  $^{\circ}\text{C}$ . **a** PVDF 20% cooled at RT, **b** PVDF 50% cooled at RT, **c** PVDF 20% quenched in ice water, and **d** PVDF 20% cooled in DSC at  $-20^{\circ}\text{C}/\text{min}$ . Scale bar is 0.5  $\mu\text{m}$

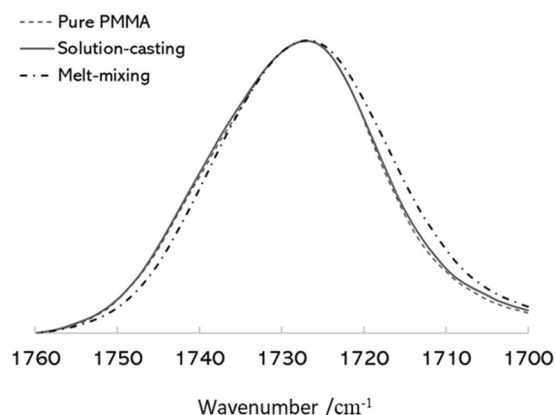
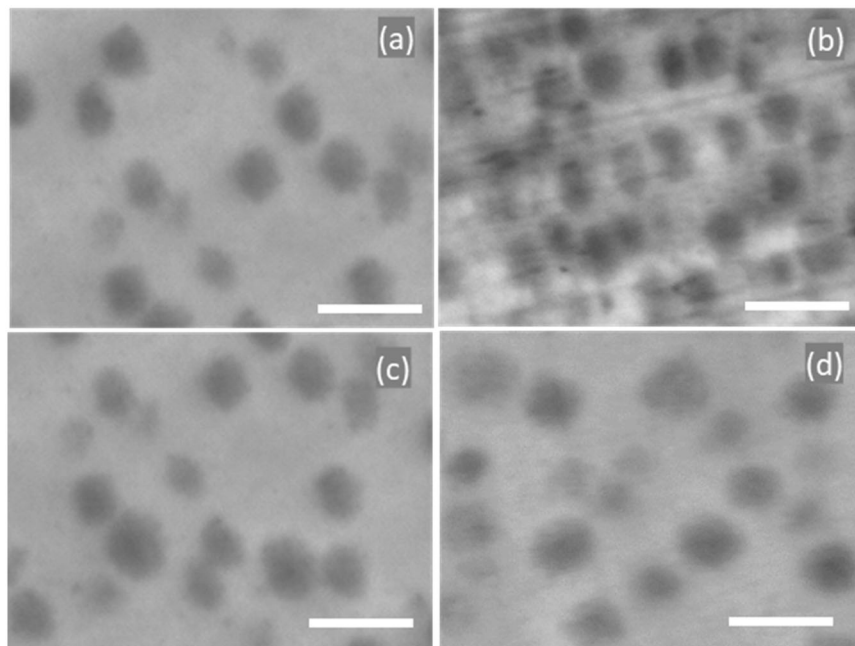


**Fig. 6** Carbonyl stretching absorption of pure PMMA and PMMA 50/PVDF 50 blends. The dotted line shows Pure PMMA, the solid line shows Solution-casting blend, and the dotted dashed line shows Melt-mixing blend

the left-hand side is a function of  $\phi_1$ . This is because  $m$  is extremely large and  $\chi_{12}$  is inherent for each polymer pair under certain conditions. This is supported by the DSC

measurements with various mixing ratios, i.e., varying  $\phi_1$ . However, it is not clear why the degree of melting point depression varies with  $\phi_1$ . What we focused on was the size of the interface regions between PMMA and PVDF where they contact and can interact with each other. The size of the interface regions of the sea-island structure in two-dimensional images, such as in this study, corresponds to the perimeter of the island. The length of the perimeter changes with the area of the islands; thus, it needs to be normalized. The value of the perimeter divided by the area is always constant, regardless of the number of islands inside the field of view, as long as the size of the islands is constant, and they are not in contact with each other. Fig. 7 shows this ratio, the perimeter divided by the area of the dark contrasts, which corresponds to PVDF domains calculated by image analysis of the STEM images of each blend. The analysis was performed on four images acquired in the size range of 100–150  $\mu\text{m}^2$ , and for the sake of analysis, the contrasts between dark and bright are reversed from the original images (see Figs. S2–S4 in Supporting

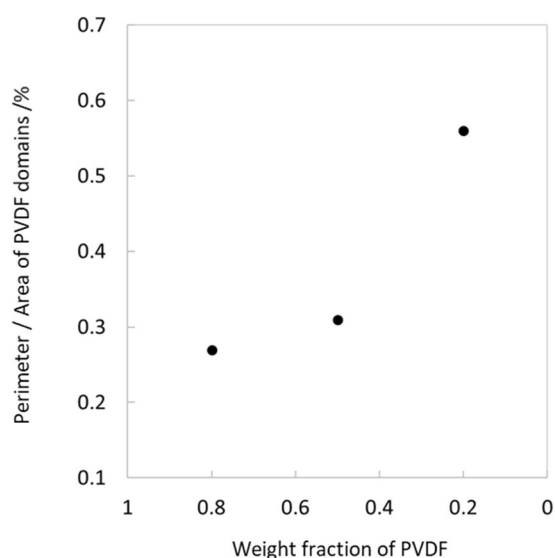


**Fig. 7** Dependence of the perimeter divided by the area of PVDF domains on the weight fraction of PVDF. The perimeter and area are calculated by image analysis

Information). As a result, the perimeters varied with the mixing ratio. The original STEM images in Fig. 4 show that the periodicity of the structures is the same regardless of the PVDF ratio. However, as the mixing ratio of PVDF increased, PVDF in the form of connected islands became more prominent. This connectivity is the cause of the decrease in the perimeters. Next, to clarify the relationship in-between, the melting point of each blend is plotted against the perimeter/area and shown in Fig. 8. The curve of the plots is almost the same as that shown in Fig. 2, where the horizontal axis is the weight fraction of PVDF. This is evidence that the size of the interface regions is closely related to the melting point depression.

Next, we discuss a complex behavior that cannot be described in the single word “melting point depression”, especially in blends with low PVDF ratios of 20 and 50%. The presence of an endothermic peak appears at a temperature lower than the main endothermic peak of each sample, as mentioned above. In Fig. 9, the melting peaks of PVDF for each blend are shown after normalization by the peak top values as well as the baseline correction. Of note, the endothermic peak at a temperature lower than the main melting peak is indicated by the arrows. Furthermore, the intensity of this peak increases as the ratio of PVDF decreases. The existence of this peak and its origin have not been mentioned in previous studies, and the origin of this peak is discussed in correlation with the newly visualized nanostructure for the first time.

First, the most convincing phenomenon suggested by the low-temperature endothermic peak is the melting of “finer crystalline PVDF. However, we would like to touch on the other possibilities as well, unraveling past research

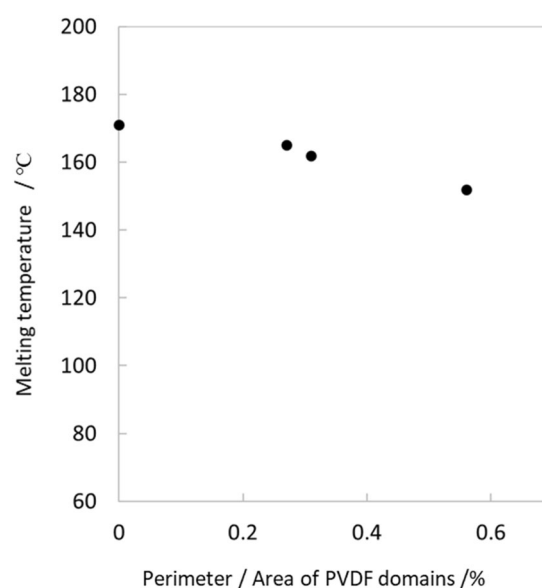


**Fig. 8** Dependence of melting temperature ( $T_m$ ) of the solution-casting blends on the perimeter divided by the area of PVDF domains. The plots are similar to Fig. 2 with PVDF weight fraction on the horizontal axis

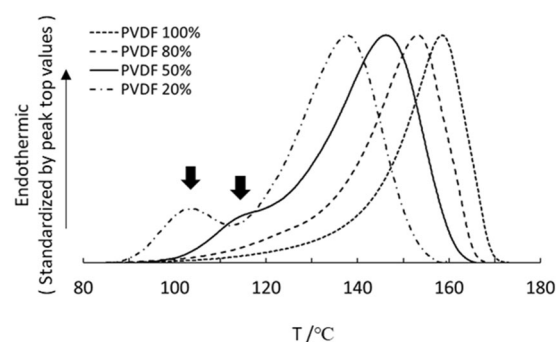


**Fig. 9** Melting peaks of solution-casting PVDF and PMMA/PVDF blends. Baseline corrected and standardized by peak top value. The arrows indicate the low-temperature melting peaks that we are focusing on

examples. In other words, it is necessary to confirm whether the low-temperature endothermic peaks could be due to phenomena other than the melting of crystalline PVDF. If this peak is not caused by melting, there are two possibilities. The first is the glass transition temperature,  $T_g$ , of the blend. The  $T_g$  values of PMMA and PVDF used in this experiment were 97 °C and −40 °C, respectively [31]. The  $T_g$  of the blend varies between the  $T_g$  of each depending on the mixing ratio and miscibility. Thus, the  $T_g$  of the blend is expected to be clearly lower than the  $T_g$  of PMMA, 97 °C. In fact, as shown in Fig. 10, thermograms of the low-temperature range, the glass transition occurs at even lower temperatures than the low-temperature endothermic peaks shown by the arrows. In these blends, the glass transition occurs very slowly, making it difficult to distinguish the

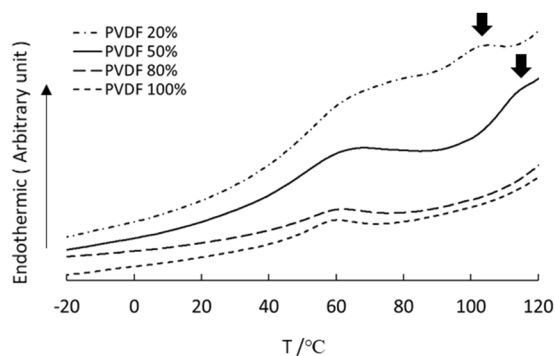


**Fig. 10** Thermograms in the low temperature range of solution-casting PVDF and PMMA/PVDF blends. The arrows indicate the low-temperature melting peaks that we are focusing on

exact positions. The exception is the blend with PVDF 20%, and it is judged that  $T_g$  exists at  $\sim 30\text{--}40\text{ }^\circ\text{C}$ . The second possibility is the endothermic peak at  $\sim 60\text{ }^\circ\text{C}$ , which is known by several previous studies to be peculiarly exhibited in PVDF. The origin is not clear, while the following possibilities have been proposed [32]: upper glass transition [31], reorganization within conformationally disordered crystals [33], molecular motions corresponding to relaxation in the crystalline/amorphous interface [34], and melting of paracrystalline domains [35]. However, this peak is observed in this experiment at  $60\text{ }^\circ\text{C}$ , which is completely different from the low-temperature endothermic peak. Although the assignment of the peak at  $60\text{ }^\circ\text{C}$  is out of our scope, we now conclude that these two possibilities are excluded.

From the viewpoint of the low-temperature melting peak observed in DSC measurements, there have been similar studies in the past. Poly(butylene succinate) possesses a low-temperature endothermic peak similar to that in this experiment, and its origin has been discussed [36, 37]. These studies lead to the conclusion that in nonisothermal crystallization from melts, especially when the cooling rate is large, components that melt at low temperatures are produced. This occurs due to the low thermal stability of the crystallites. The findings in these studies do not directly apply to our study because the mixing and crystallization processes are different. However, the fact that crystals in different states can be produced from a single polymer provides some support for the low-temperature melting peak observed in this study. It is difficult to further verify its origin from the thermogram alone. However, further discussion can be made by correlating the results of LV-STEM observations as follows.

The area of the domains was calculated from the binary images used to measure the perimeter length earlier and are shown in Table 1. In the blend with 80% PVDF, the area ratio of dark contrast was almost the same as the PVDF ratio. However, in the blend with PVDF 50%, only  $\sim 70\%$  of

**Table 1** Area ratio of PVDF domains calculated by image analysis of STEM images for various solution-casting blends

PVDF weight fraction (%)	Analysis number	Area ratio of PVDF domains (%)
20	n1	10
	n2	10
	n3	11
	n4	11
50	n1	36
	n2	32
	n3	39
	n4	38
80	n1	78
	n2	78
	n3	75
	n4	77

the PVDF ratio appears as the area ratio of dark contrasts, and in the blend with PVDF 20%, only approximately half of the PVDF ratio appears as the area ratio of dark contrasts. Two aspects are necessary for the discussion based on these results. First, it is worth repeating that almost all crystallizable PVDF in the blend was crystallized regardless of the PVDF ratio, based on Fig. 3. This indicates that the area ratio must be equal to the PVDF ratio regardless of the PVDF ratio. Second, PVDF is a semicrystalline polymer. In our measurement, the melting enthalpy of pure PVDF is  $58.1\text{ J/g}$ , and the corresponding crystallinity becomes  $55\%$  based on  $104.1\text{ J/g}$  of perfect crystal [34]. This means that even if all crystallizable PVDF is crystallized, it contains a  $45\%$  amorphous component. If this crystallinity is directly multiplied by the PVDF ratio of the blend with PVDF 80%, the dark contrast ratio of 77 would be too high, assuming that only the crystallized area was observed. However, this statement is negated in terms of the spatial resolution of STEM and the image analysis, as explained below.

Figure 4a shows that there are even more light and dark contrasts in the dark domains corresponding to PVDF (see Fig. S5 in the supplementary information, more high-resolution images). We speculate that these light and dark contrasts are generated in accordance with the amorphous and crystalline regions of PVDF. The amorphous component of semicrystalline polymers is typically located at interlamellar or interfibrillar areas. Their scales vary depending on the composition and the process of crystallization. For example, a value of  $2.5\text{ nm}$  for the interlamellar thickness was reported for pure PVDF [38]. The size of the interfibrillar region is measured to be several to several tens of nm, based on the image in Fig. 4a. These scales are very small compared to the spatial resolution of both STEM and image analysis. As a result, both amorphous regions together with the crystalline region of



PVDF are incorporated into the dark contrast area. Thus, the dark contrast ratio of 77% reproduced well the PVDF composition of 80%. In addition, FT-IR measurements show that there is no hydrogen bonding between PMMA and PVDF in the solution-casting blend, meaning that amorphous PVDF does not interact with PMMA in the blends. This suggests that amorphous PVDF is only present in the interlamellar and interfibrillar regions of the crystalline PVDF domains.

We can conclude that the dark contrast area contains all PVDF components for the blend of PVDF 80%. However, the data for both 20 and 50% show the deviation. This deviation indicates the presence of crystalline PVDF that is not visible in LV-STEM, which is a reasonable interpretation in terms of the resultant spatial resolution due to our experimental conditions. The thickness of the ultrathin specimens used in this observation was approximately 100 nm, which is a typical thickness for polymeric materials. Then, it is common sense that any objects consisting of light elements with sizes extremely smaller than the specimen thickness cannot be visualized by TEM.

The abovementioned result suggests the presence of fine crystalline PVDF that cannot be visualized by LV-STEM in blends with low PVDF ratios and that these crystals increase in correlation with a decrease in PVDF ratio. This can be related to the presence of crystalline PVDF with a low-temperature melting peak observed by DSC. First, this low-melting crystalline PVDF tends to increase with decreasing PVDF ratio, as mentioned above, which is similar to the increasing tendency of fine crystalline PVDF by LV-STEM. The low melting point indicates that the crystals are fine crystals with thin lamellar thicknesses, implying that both the low-melting crystalline PVDF evidenced by thermograms and the invisible fine crystals are identical to each other. The increase in this invisible component with decreasing PVDF ratio in the blend is estimated to be due to the  $T_g$  of the blend.  $T_g$  increases with a decrease in the PVDF ratio; at high  $T_g$  there is a decrease in molecular mobility. This means that as the PVDF ratio decreases, the mobility of the PVDF molecules decreases, and as a result, they do not gain the necessary mobility to form domains.

### Melt-mixing samples

The amorphous state shown by the blends with PVDF 50 and 20% in DSC measurements is consistent with a previous study [2]. The new finding in this study is the fine sea-island structure visualized by LV-STEM. First, this structure was also observed in the ice-water quenched sample, as shown in Fig. 5c, and therefore can be judged to reflect the melt miscibility of PMMA and PVDF. As mentioned above, PMMA and PVDF are completely mixed in the molten

state, which can be described as molecular miscibility, but from the nanoscale point of view, it is newly clarified that they form a fine heterogeneous structure.

Next, in discussing the composition of each component and the origin of structure formation, we consider the presence of an endothermic peak at  $\sim 60^\circ\text{C}$ , as previously mentioned. In other words, it is necessary to check whether the islands seen in LV-STEM observations are relevant to paracrystalline PVDF or other heterogeneous structures. For this purpose, after the DSC measurement, the sample was cooled from  $200^\circ\text{C}$  to room temperature at  $-20^\circ\text{C}/\text{min}$  in DSC and measured again at  $10^\circ\text{C}/\text{min}$ . In this 2nd run measurement, the endothermic peak at  $\sim 60^\circ\text{C}$  disappeared (see Fig. S6 in Supplementary Information), which was also confirmed in a previous study [32]. The image in Fig. 5a was obtained for the specimen cooled at RT, which corresponds to the 1st scan, i.e., the blend with an endothermic peak near  $60^\circ\text{C}$ . In contrast, the image in Fig. 5d was obtained for the specimen with cooling at  $-20^\circ\text{C}/\text{min}$  in DSC, which means a 2nd scan, where similar sea island structures were visible. This fact excludes any possibility that paracrystalline PVDF or other heterogeneous structures are the cause of the fine sea-island structure observed in this study.

We are interested in the compositional attribution of islands and seas, as well as their formation factors. For this reason, the area ratio of islands with dark contrast was determined by image analysis as in the solution casting blend. Because the microstructure here is highly reproducible, the analysis was performed only on three images with a smaller size of  $5\ \mu\text{m}^2$  (see Fig. S7 in Supplementary Information). The obtained results show that the average dark contrast area of the blend with 20% PVDF is 28%, which is larger than the ratio of PVDF in the blend. This, at least, indicates that the composition of the island is not pure PVDF but a mixture with PMMA. Next, to determine the presence or absence of PVDF in the sea region, we measured the number of islands in blends containing 20 and 50% PVDF (see Figs. S8 and S9 in Supplementary Information). Here, the contrast difference between the islands and the sea in the PVDF 50% blend was small and could not be binarized. Therefore, the number of islands was used instead. The number of islands in the same  $14\ \mu\text{m}^2$  size images were  $\sim 78$  and 129, respectively. These numbers cannot simply be explained by the value of the PVDF ratio: 20 to 50% of the PVDF ratio is a 2.5-fold increase, whereas 78–129 islands are only a 1.6-fold increase. This means that PVDF is present in the sea region of at least the PVDF 50% blend. Furthermore, based on the similarity of the structure, we believe that PVDF is also present in the sea region of the 20% PVDF blend.

Next, we discuss the state of PVDF molecules in this fine sea island structure and the factors responsible for its

formation. The PVDF used in this study has an  $M_w$  of ~500,000, and its single molecular chain length is considered to be ~2  $\mu\text{m}$ . This is derived from a value of ~3 nm/12.5 monomer, which was obtained by computational molecular modeling in a previous study [39]. The size of the island identified in this study was ~300 nm and did not deviate from the expected size of the random coil formed from this molecular chain. This hypothesis is supported by the fact that the size of the islands does not change between the blends with PVDF ratios of 50 and 20%. Furthermore, this idea is strengthened by the similar island size of crystalline PVDF seen in solution-casting blends, which is ~200 nm. As shown earlier, in solution-casting blends, PMMA and PVDF exist in an incompatible manner, i.e., there is no PMMA in the islands. Therefore, the slightly smaller size for solution-casting blends is consistent with our hypothesis. To further support this hypothesis, validation using PVDF with different molecular weights is needed.

## Conclusion

By applying LV-STEM to PMMA/PVDF blends, their nanoscale internal structures, never seen before, were visualized. By performing image analysis on these structures and correlating them with DSC and FT-IR measurements, the following three new insights were obtained. First, the size of interface regions is closely related to the melting point depression. Second, the low-temperature melting peaks of DSC observed in solution-casting blends, especially with low PVDF ratios, originate from fine PVDF crystals that are difficult to observe even by electron microscopy. The last insight is for melt-mixing blends where PVDF is in an amorphous state, meaning that PMMA and PVDF are miscible. Even in this state, a fine heterogeneous structure was observed in blends, which is the visualization of the molecular miscibility of PMMA and PVDF for the first time.

## Compliance with ethical standards

**Conflict of interest** The authors declare no competing interests.

**Publisher's note** Springer Nature remains neutral with regard to jurisdictional claims in published maps and institutional affiliations.

## References

- Daimon K, Ninomiya M. EA-Eco toner. Fuji Xerox Technical Reports. 2011.
- Noland JS, Hsu NN-C, Saxon R, Schmitt JM. Compatible high polymers; poly (vinylidene fluoride) blends with homopolymers of methyl and ethyl methacrylate. Multicompon Polym Syst. 1971. <https://doi.org/10.1021/ba-1971-0099.ch002>
- Nishi T, Wang TT. Melting point depression and kinetic effects of cooling on crystallization in poly (vinylidene fluoride)-poly (methyl methacrylate) mixtures. *Macromolecules*. 1975. <https://doi.org/10.1021/ma60048a040>
- Aid S, Eddhahak A, Khelladi S, Ortega Z, Chaabani S, Tcharkhtchi A. On the miscibility of PVDF/PMMA polymer blends: thermodynamics, experimental and numerical investigations. *Polym Test*. 2019. <https://doi.org/10.1016/j.polymertesting.2018.11.036>
- Shi Z, Ma X, Zhao G, Wang G, Zhang L, Li B. Fabrication of high porosity nanocellular polymer foams based on PMMA/PVDF blends. *Mater Des*. 2020. <https://doi.org/10.1016/j.matdes.2020.109002>
- Sasaki H, Bala PK, Yoshida H, Ito E. Miscibility of PVDF/PMMA blends examined by crystallization dynamics. *Polymer*. 1995. [https://doi.org/10.1016/0032-3861\(95\)99296-7](https://doi.org/10.1016/0032-3861(95)99296-7)
- Yoshida H. Structure formation of PVDF/PMMA blends studied. *J Therm Anal*. 1997. <https://doi.org/10.1007/BF01987426>
- Horibe H, Hosokawa Y, Oshiro H, Sasaki Y, Takahashi S, Kono A, et al. Effect of heat-treatment temperature after polymer melt and blending ratio on the crystalline structure of PVDF in a PVDF/PMMA blend. *Polym J*. 2013. <https://doi.org/10.1038/pj.2013.53>
- Kwei TK, Patterson GD, Wang TT. Compatibility in mixtures of poly (vinylidene fluoride) and poly (ethyl methacrylate). *Macromolecules*. 1976. <https://doi.org/10.1021/ma60053a018>
- Wang TT, Nishi T. Spherulitic Crystallization in Compatible Blends of Poly (vinylidene fluoride) and Poly (methyl methacrylate). *Macromolecules*. 1977. <https://doi.org/10.1021/ma60056a034>
- Roerdink E, Challa G. Influence of tacticity of poly (methyl methacrylate) on the compatibility with poly (vinylidene fluoride). *Polymer*. 1978. [https://doi.org/10.1016/0032-3861\(78\)90034-4](https://doi.org/10.1016/0032-3861(78)90034-4)
- Morra BS, Stein RS. Morphological studies of poly(vinylidene fluoride) and its blends with poly(methyl methacrylate). *J Polym Sci: Polym Phys Edition*. 1982. <https://doi.org/10.1002/pol.1982.180201208>
- Okabe Y, Murakami H, Osaka N, Saito H, Inoue T. Morphology development and exclusion of noncrystalline polymer during crystallization in PVDF/PMMA blends. *Polymer*. 2010. <https://doi.org/10.1016/j.polymer.2010.01.055>
- Hirata Y, Kotaka T. Phase separation and viscoelastic behavior of semicompatible polymer blends: poly (vinylidene fluoride)/poly (methyl methacrylate) system. *Polym J*. 1981. <https://doi.org/10.1295/polymj.13.273>
- Zhang Y, Zuo M, Song Y, Yan X, Zheng Q. Dynamic rheology and dielectric relaxation of poly (vinylidene fluoride)/poly (methyl methacrylate) blends. *Compos Sci Technol*. 2015. <https://doi.org/10.1016/j.compscitech.2014.10.024>
- Douglass DC, McBrierty VJ. Compatibility in PVDF/PMMA and PVDF/PEMA blends as studied by pulsed NMR. *Macromolecules*. 1978. <https://doi.org/10.1021/ma60064a030>
- Papavoine CHM, Maas WEJR, Veeman WS, Buning GHW, Vankan JMJ. Triple-resonance proton-fluorine-19-carbon-13 CPMAS NMR study on the crystallization behavior of the PMMA/poly(vinylidene fluoride) 60/40 blend. *Macromolecules*. 1993. <https://doi.org/10.1021/ma00076a0046>
- Léonard C, Halary JL, Monnerie L. Hydrogen bonding in PMMA-fluorinated polymer blends: FTi.r. investigations using ester model molecules. *Polymer*. 1985. [https://doi.org/10.1016/0032-3861\(85\)90084-9](https://doi.org/10.1016/0032-3861(85)90084-9)
- Coleman MM, Painter PC. Hydrogen bonded polymer blends. *Prog Polym Sci*. 1995. [https://doi.org/10.1016/0079-6700\(94\)00038-4](https://doi.org/10.1016/0079-6700(94)00038-4)
- Gregorio R Jr, Borges DS. Effect of crystallization rate on the formation of the polymorphs of solution cast poly (vinylidene

- fluoride). *Polymer*. 2008. <https://doi.org/10.1016/j.polymer.2008.07.010>
21. Hahn B, Wendorff J, Yoon DY. Dielectric relaxation of the crystal-amorphous interphase in poly (vinylidene fluoride) and its blends with poly (methyl methacrylate). *Macromolecules*. 1985. <https://doi.org/10.1021/ma00146a024>
  22. Hahn BR, Herrmann-Schönherr O, Wendorff JH. Evidence for a crystal-amorphous interphase in PVDF and PVDF/PMMA blends. *Polymer*. 1987. [https://doi.org/10.1016/0032-3861\(87\)90404-6](https://doi.org/10.1016/0032-3861(87)90404-6)
  23. Ma W, Zhang J, Wang X, Wang S. Effect of PMMA on crystallization behavior and hydrophilicity of poly(vinylidene fluoride)/poly(methyl methacrylate) blend prepared in semi-dilute solutions. *Appl Surf Sci*. 2007. <https://doi.org/10.1016/j.apsusc.2007.04.001>
  24. Libera MR, Egerton RF. Advances in the transmission electron microscopy of polymers. *Polym Microsc*. 2010. <https://doi.org/10.1080/15583724.2010.493256>
  25. Hoffman JD, Weeks JJ. Melting process and the equilibrium melting temperature of polychlorotrifluoroethylene. *J Res Nat Bur Stand Sect A*. 1962;66A:13–28.
  26. Neidhöfer M, Beaume F, Ibos L, Bernès A, Lacabanne C. Structural evolution of PVDF during storage or annealing. *Polymer*. 2004. <https://doi.org/10.1016/j.polymer.2003.12.066>
  27. Jo WH, Lee MR, Min BG, Lee MS. Miscibility of poly(ether imide)/poly(ethylene terephthalate). *Polym Bull*. 1994. <https://doi.org/10.1007/BF00313482>
  28. Qiu Z, Yan C, Lu J, Yang W, Ikehara T, Nishi T. Various crystalline morphology of poly(butylene succinate-co-butylene adipate) in its miscible blends with poly(vinylidene fluoride). *J Phys Chem*. 2007. <https://doi.org/10.1021/jp067606f>
  29. Wiranidchapon C, Rades T, Kulvanich P, Tucker IG. Method of preparation does not affect the miscibility between steroid hormone and polymethacrylate. *Thermochim Acta*. 2009. <https://doi.org/10.1016/j.tca.2008.12.013>
  30. Chenyang X, Mengmeng Z, Liping Z, Jichun Y, Xiaojun C, Yongjin L. Ionic liquid modified poly(vinylidene fluoride): crystalline structures, miscibility, and physical properties. *Polym Chem*. 2013. <https://doi.org/10.1039/C3PY00466J>
  31. Leonard C, Halary JL, Monnerie L, Micheron F. DSC studies on the transitions in poly (vinylidene fluoride) and some related copolymers. *Polym Bull*. 1984. <https://doi.org/10.1007/BF00258030>
  32. Merlini C, Barra GMO, Araujo TM, Pegoretti A. Electrically pressure sensitive poly(vinylidene fluoride)/polypyrrole electrospun mats. *RSC Adv*. 2014. <https://doi.org/10.1039/C4RA01058B>
  33. Loufakis K, Wunderlich B. Thermal analysis of the conformational disorder in semicrystalline poly (vinylidene fluoride) and poly(trifluoroethylene). *Macromolecules*. 1987. <https://doi.org/10.1021/ma00176a026>
  34. Teyssedre G, Bernes A, Lacabanne C. Influence of the crystalline phase on the molecular mobility of PVDF. *J Polym Sci: Part B Polym Phys*. 1993. <https://doi.org/10.1002/polb.1993.090311316>
  35. Nabata Y. Molecular motion in form II poly (vinylidene fluoride). *Jpn J Appl Phys*. 1990. <https://doi.org/10.1143/JJAP.29.2782>
  36. Yasuniwa M, Satou T. Multiple melting behavior of poly(butylene succinate). I. Thermal analysis of melt-crystallized samples. *J Polym Sci: Part B Polym Phys*. 2002. <https://doi.org/10.1002/polb.10298>
  37. Qiu Z, Komura M, Ikehara T, Nishi T. DSC and TMDSC study of melting behaviour of poly(butylene succinate) and poly(ethylene succinate). *Polymer*. 2003. <https://doi.org/10.1016/j.polymer.2003.10.045>
  38. Nakagawa K, Ishida Y. Dielectric relaxation and molecular motions in polyvinylidene fluoride with crystal form II. *J Polym Sci: Part B Polym Phys Ed*. 1973. <https://doi.org/10.1002/pol.1973.180110804>
  39. Bystrov VS, Paramonova EV, Bdikin IK, Bystrova AV, Pullar RC, Kholkin AL. Molecular modeling of the piezoelectric effect in the ferroelectric polymer poly (vinylidene fluoride) (PVDF). *J Mol Model*. 2013. <https://doi.org/10.1007/s00894-013-1891-z>